Short Communication

Effect of solid-solution temperature on microstructure of incoloy825 alloy and its corrosion behavior in a polluted marine environment

Min Zhu[*], *Zhongping Le, Yongfeng Yuan, Shaoyi Guo, Jian Zhou*

School of Mechanical Engineering & Automation, Zhejiang Sci-Tech University, Hangzhou 310018, PR China
[*]E-mail: zmii666@126.com

Effects of solid-solution temperature on microstructure and its corrosion behavior of incoloy825 alloy in a polluted marine environment were investigated by electrochemical tests and periodic wet-dry cycle test. The corrosion resistance of alloy sample improves with the rise of solid-solution temperature. The corrosion law of the alloy is closely related with different microstructures. The increase in grain size and the amount of Ti(C,N) precipitates can decrease the corrosion degree. The electrochemical parameters of R_f, R_{ct} and i_p indicate that the passive films formed on the samples with different microstructures have different protective property. All samples mainly exhibit the feather of localized corrosion, and the degree of localized corrosion significantly reduces with an increase in the solid-solution temperature.

Keywords: Solid-solution temperature; Corrosion behavior; Microstructure; Localized corrosion

1. INTRODUCTION

Incoloy825 alloy has been used in many areas such as marine engineering, chemical engineering and aviation field, which is due to the superior corrosion resistance, mechanical property and processability[1]. So far, the relevant researches[2-4] of the alloy are mainly concerned on welding performance, wear resistance, microstructure, and so on. Very few reports have been involved on the corrosion resistance[5-7]. Tan[8] has reported the intergranular corrosion behavior of aged alloy. The results indicated that aged temperature and time greatly affected the sensitization degree and the corresponding corrosion status. Li[9] found that 825 alloy had a greater corrosion resistance because of the higher chromium content, compared with that of 600 alloy.

In the application of actual engineering, the welding joints with complex microstructure are

extensively existed in various engineering structures. In the welding process, different areas within the joint exhibit various temperatures. And the difference in temperature can cause the evolution of microstructure in the welded joint region. At present, the related research about the effect of solid-solution temperature on the corrosion behavior of incolo825 alloy has not been reported. In marine environment, the spray splash zone is a hostile environment condition for the anticorrosion resistance of employed material. The results of many literatures[10-12] indicated that the severe corrosion status in this region was due to the condition characteristics of we-dry alternation. While the welded joint of incoloy825 alloy is used in the spray splash zone, its corrosion behavior may be significantly different. Based on this point, in this work, the influence of solid-solution temperature on microstructure and corrosion behavior of incoloy825 alloy in a polluted marine environment containing $NaHSO_3$ is investigated by electrochemical measurements and periodic wet/dry cycle corrosion test.

2. EXPERIMENTAL

The chemical composition of incoloy825 alloy is (wt.%): Ni 46.00, Cr 23.50, Cu 3.00, Ti 1.20, Mo 3.50, Mn 1.00, Si 0.50, P 0.02, C 0.03, S 0.01 and Fe balance. In the welding process, different areas within the joint may experience various temperatures, and generates the complex microstructure. Therefore, the simulated microstructure of weld joint of incoloy825 alloy was fabricated by heat treatment of different solid-solution temperatures. The heat treatment was as follow: heating to different temperatures of 1000°C, 1070°C and 1150°C for holding time of 40 min in the air and then cooling down to indoor temperature in the water. The sample treated by heat treatment (10 mm ×10 mm × 3mm) was embedded in epoxy resin, leaving an exposed region of 1 cm^2 as the working surface. Then the samples were orderly grinded, polished, rinsed, and finally dried. The microstructure of samples was observed by scanning electron microscope (SEM) and the attached Energy Dispersive Spectrometer (EDS). And the grain size of samples was obtained by quantitative metallography method. The polluted seawater was prepared by adding 0.05M $NaHSO_3$ to 3.5% NaCl solution. The test temperature was kept constant at 30°C.

The tests were performed through periodic wet/dry cycle corrosion system. One period was 1h, the samples were immerged into the solution bath in the wet step for 12 min, and kept in oven for 48 min during the dry process. The relative humidity (RH) was maintained at 90%. After 1 day of testing, the specimens were taken out for electrochemical tests. The tests were carried out via a conventional three-electrode cell using the CHI660E electrochemical workstation system. The alloy specimen was acted as working electrode, a saturated calomel electrode (SCE) as reference electrode, and a platinum sheet as counter electrode. The open circuit potential (OCP) of the samples was tested for 30 min. Then EIS test was conducted at OCP in a frequency range from 100 kHz to 10 mHz with the disturbance AC signal amplitude of 10 mV. The potentiodynamic polarization curve was measured at a scanning rate of 0.5 mV/s from -0.9 V (vs SCE) to 0.5 V (vs SCE).

Before the test, the specimen was cleaned, dried and weighed. After the periodic wet/dry cycle corrosion test of 10 days, the corrosion product formed on the sample was removed completely. Whereafter, the samples were washed, dried, and weighed, and then the corrosion rate of alloy samples

treated at different solid-solution temperatures was calculated according to the weight-loss analysis. The corrosion morphology of alloy samples was observed via SEM.
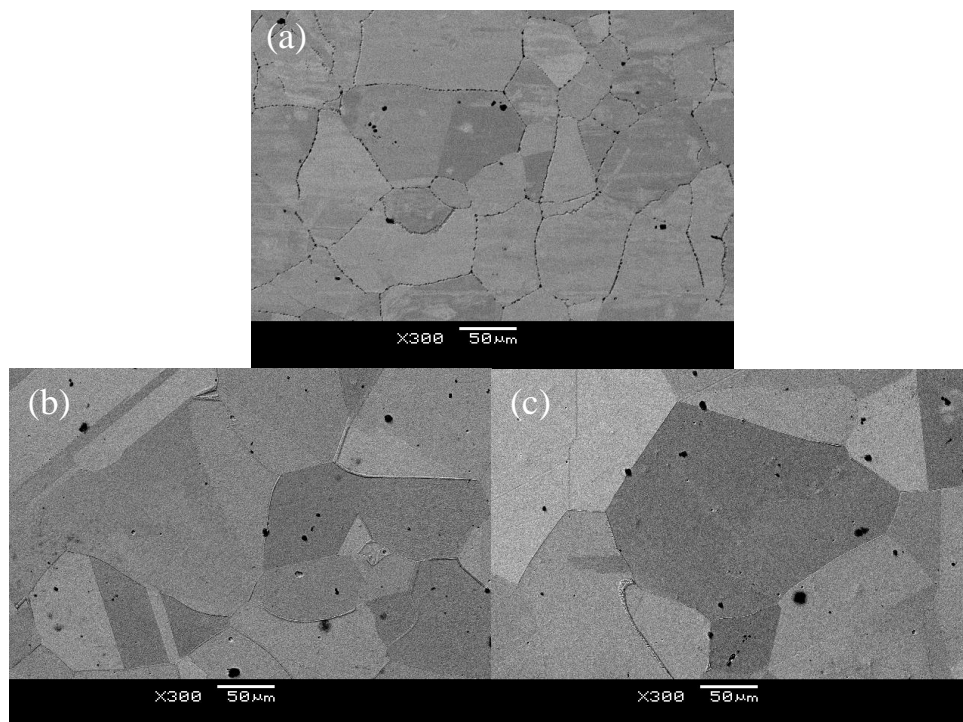
3. RESULTS

Figure 1. Microstructure of incoloy825 alloy samples treated at different solid-solution temperatures for 40min (a) 1000℃； (b) 1070℃； (c) 1150℃

Figure 1 shows the microstructure of incoloy825 alloy samples treated at different solid-solution temperatures for 40min. The samples consist of single austenite phase (Υ) and black granular precipitate (Ti(C,N)). After the treatment, the average grain sizes of samples treated at 1000℃, 1070℃ and 1150℃ are 11μm, 40μm and 250μm respectively. That is, the grain size increases with an increase in solid-solution temperature, especially at the temperature range of 1070℃-1150℃. Moreover, the precipitation of Ti(C,N) also increases. And the EDS result demonstrates the presence of Ti(C,N), which is shown in Figure 2.
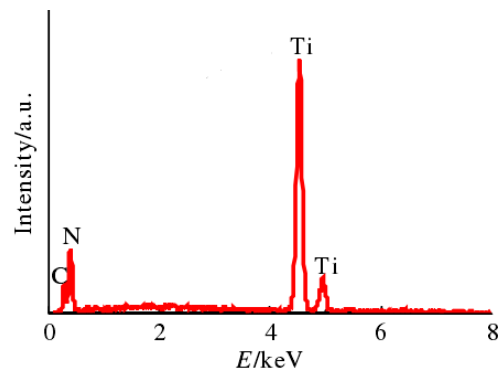
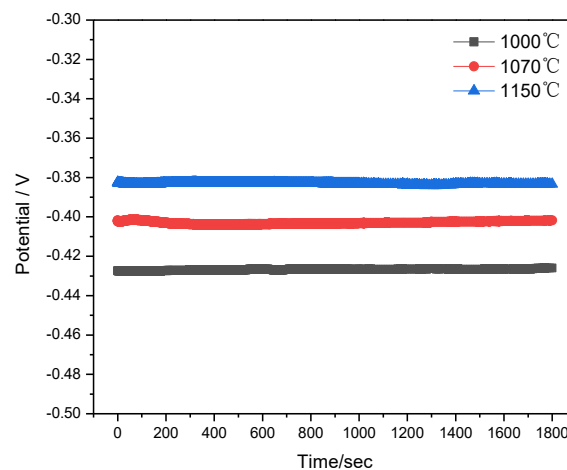**Figure 2.** EDS result of precipitates of Ti(C,N) within microstructure

Figure 3. Open circuit potential of incoloy825 alloy samples treated at different solid-solution temperatures

Figure 3 shows the open circuit potential (OCP) of alloy samples treated at different solid-solution temperatures. With increasing test time, all curves reveal that the OCP holds a relatively stable status with the augment of testing time. In addition, the OCP shifts positively as an increased temperature. That is, the sample treated at 1150°C has the most positive OCP value, which suggests that the difference in solid-solution temperature could affect the corrosion tendency. The higher the solution temperature, the smaller the corrosion tendency is.

Figure 4 shows the impedance spectra of alloy samples treated at different solid-solution temperatures in the polluted seawater. As showed in Fig.4, the curves exhibit the capacitive arc characteristic, with different diameters of impedance semicircles. The capacitive loop diameter of sample increases with the increase of solid-solution temperature. This means that alloy samples treated at different temperatures possess different corrosion resistance.
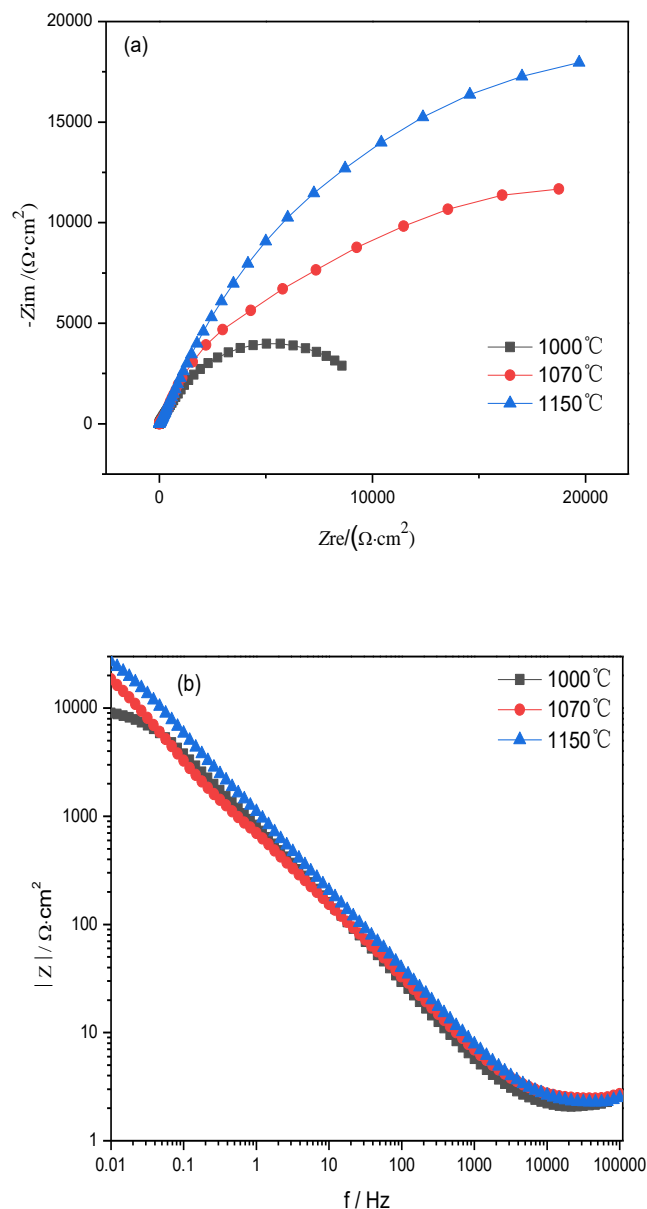
Figure 4. Impedance spectra of incoloy825 alloy samples treated at different solid-solution temperatures in the polluted seawater (a) Nyquist plot, (b) Bode diagram.

In the low frequency zone of Fig.4b, the |Z| value of alloy sample treated at 1150℃ is the maximum, followed by 1070℃, and the sample treated at 1000℃ exhibits the lowest value. The larger the |Z| value, the better the corrosion resistance is [13]. Thus, the alloy specimen treated at 1150℃ has the optimum corrosion resistance, comparing with those of the lower temperatures.

Using the equivalent circuit $R_s(Q_fR_f)(Q_{dl}R_{ct})$ to fit the impedance spectroscopy. Among them, R_s is the solution resistance, and Q_f represents the capacitance of the passive film, coupled with the resistance of passive film R_f. Q_{dl} represents the non-ideal capacitance of double layer, and R_{ct} is the charge transfer resistance [14]. As listed in Table.1, the alloy treated at different temperatures has different R_f value, suggesting that there is a difference existing in the protective performance of passive

films formed on the surface of alloy samples. Among them, the sample treated at 1150°C exhibits the largest R_f and the lowest Q_f value, which indicates that the passive film covered on the sample has the best corrosion resistance [15]. And the film on the sample treated at 1000°C exhibits the worst protective property. In addition, Tab. 1 presents that the R_{ct} value of alloy sample increases with the augment of solid-solution temperature. The larger the R_{ct} value, the greater the anti-corrosion resistance is[16-18]. Therefore, the above analysis suggests that the different temperature causes the difference in corrosion resistance, which may be related to the microstructure.

Table 1. The fitting parameters for the impedance spectra of different alloy samples.

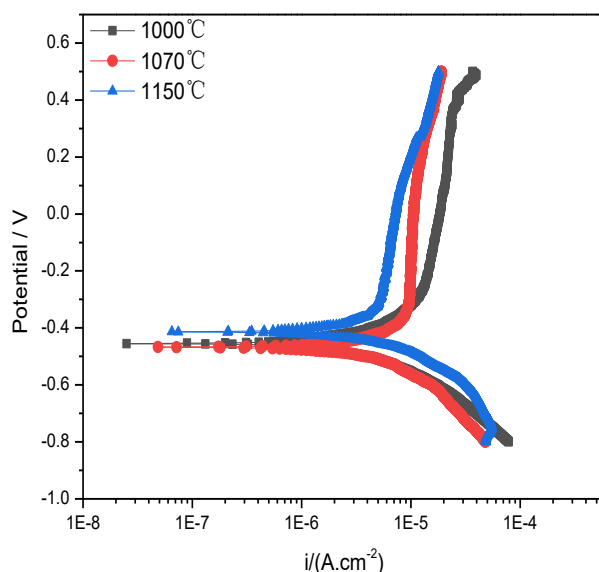| Temperature	R_s ($\Omega \cdot cm^2$)	Q_f 10^{-5}(F·cm^{-2})	n_1	R_f 10^4($\Omega \cdot cm^2$)	Q_{dl} 10^{-5}(F·cm^{-2})	n_2	R_{ct} 10^4($\Omega \cdot cm^2$)
1000°C	22.05	5.84	0.917	0.1067	4.791	0.897	0.96
1070°C	10.95	4.986	0.932	0.2166	4.301	0.925	1.568
1150°C	13.87	4.15	0.948	0.2279	3.98	0.918	2.576

Figure 5. Polarization curve of incoloy825 alloy samples treated at different solid-solution temperatures in the polluted seawater

Figure 5 reveals the polarization curves of incoloy825 alloy samples treated at different solid-temperatures in the polluted seawater. The apparent passivation characteristic is clearly observed in the analogous anode curves, which suggests that the alloy samples treated at different temperatures have the same corrosion mechanism. While the passive current density (i_p) of alloy samples treated at different temperatures is different. With the increase of solid-solution temperature, the fitted i_p value calculated from the curves of different samples are 21.8μA·cm^{-2}, 13.5μA·cm^{-2} and 9.6μA·cm^{-2} respectively. That is, i_p value declines as the increasing temperature. The smaller the i_p value, the lower the corrosion rate is. This indicates that the alloy sample treated at 1150°C has the optimal corrosion resistance, with the lowest corrosion rate, followed by 1070°C.
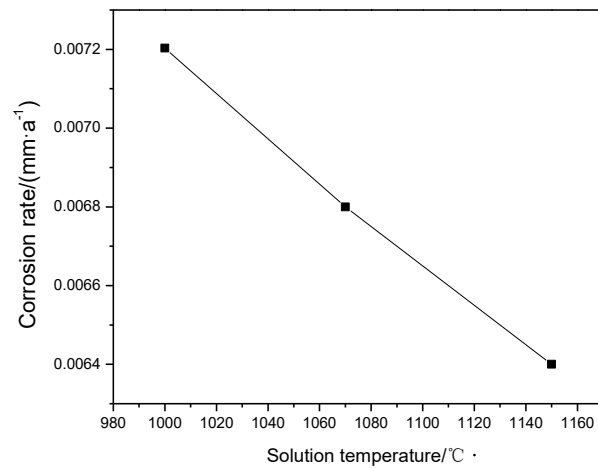
Figure 6. Corrosion rates of alloy samples treated at different solid-solution temperatures under the periodic wet/dry cycle condition for 10d

Figure 6 depicts the corrosion rates of alloy samples treated at different solid-solution temperatures under the periodic wet/dry cycle condition for 10d. The corrosion rate decreases as the increase of solid-solution temperature. This indicates that the alloy treated at 1150°C processes the greatest anti-corrosion resistance.
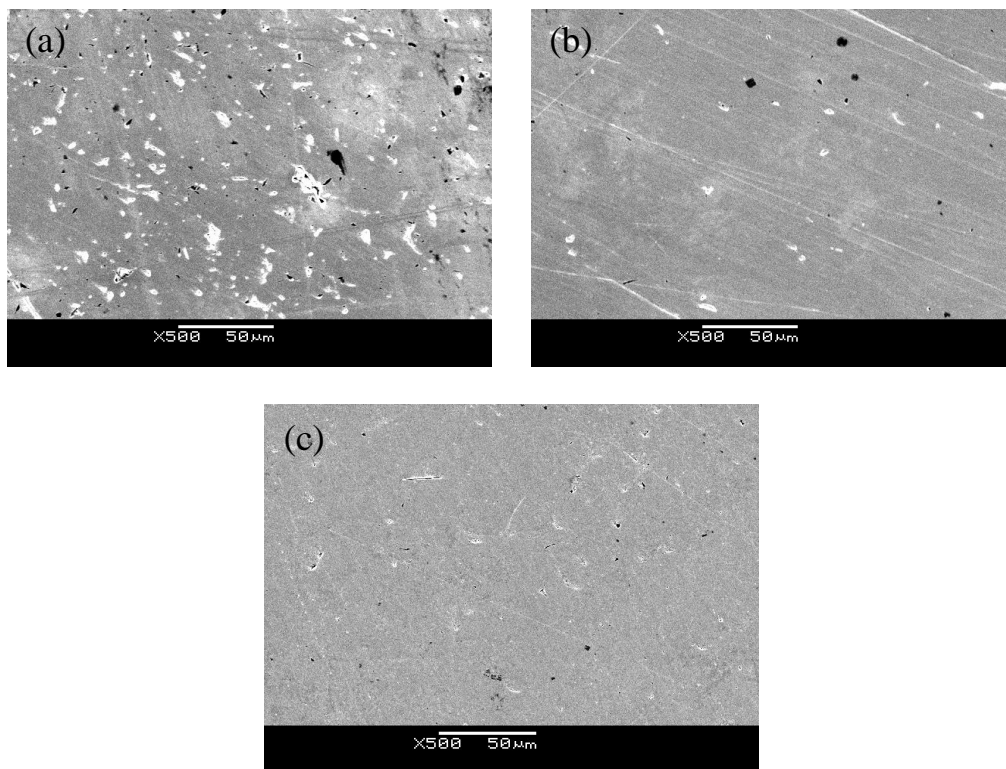

Figure 7. Corrosion morphologies of alloy samples treated at different solid-solution temperatures under the periodic wet/dry cycle condition for 10d after the removal of corrosion products
(a) 1000°C; (b) 1070°C; (c) 1150°C

Figure 7 shows the corrosion morphologies of alloy samples treated at different solid-solution temperatures under the periodic wet/dry cycle condition for 10d. All samples mainly exhibit the feather of localized corrosion. The specimen treated at 1000°C displays the most severe corrosion degree, with a mass of pits distributed on the surface. And some small-scale pits dissolve together and form the large-scale corrosion pits. Obviously, the number and size of localized corrosion significantly reduces with the increase of solid-solution temperature. Especially, for the alloy treated at 1050°C, the corrosion degree is slight, with very few pits.

According to the results of electrochemical tests and weight loss measurement, the corrosion resistance of alloy sample improves as the increase of solid-solution temperature. The corrosion law of the alloy may be related to the microstructure. As shown in Fig.1, the grain size increases with the increasing temperature. That is, the higher the temperature, the less the number of grain boundary is. Generally, the grain boundary region is prone to corrosion as the activity area [19,20]. Thus, at some extent, the increase in grain size can decrease the corrosion degree. Moreover, the precipitation of Ti(C,N) also affects the corrosion status of alloy. In the electrode reaction process, Ti(C,N) acts as the cathode due to the higher potential of 2.089V, while the alloy substrate is served as the anode because of the lower potential of -0.257V[21]. Hence, as the cathode precipitate, the existence of Ti(C,N) can effectively improve the potential of the alloy sample, and the more the number of Ti(C,N), the nobler the potential is. The OCP result can testify this point. Therefore, the difference in the microstructure leads to different corrosion behavior.

4. CONCLUSIONS

The corrosion resistance of alloy sample improves as the increase of solid-solution temperature. The corrosion law of the alloy is closely related with different microstructures. The increase in grain size and the amount of Ti(C,N) precipitates can decrease the corrosion degree. The electrochemical parameters of R_f, R_{ct} and i_p indicate that the passive films formed on the samples with different microstructures have different protective property. All samples mainly exhibit the feather of localized corrosion, and the degree of localized corrosion significantly reduces with an increase in solid-solution temperature.

References

1. R. B. Rebak and P.Crook, *Adv. Mater. Process.,* 157(2000) 37.
2. N. Sayyar, M. Shamanian and B.Niroumand, *J.Mater. Process. Tech.,* 262(2018)562.
3. J. Kangazian and M. Shamanian, *J. Manuf. Process.,* 26(2017)407.
4. L.Yang, Z.Y.Geng, M.C. Zhang and J.X.Dong, *Proc. Eng.,* 27(2012)997.
5. S. A.Al-Fozan and A. U.Malik, *Desalination*, 228(2008)61.
6. Z.F.Yin, W.Z.Zhao, W.Y.Lai and X.H.Zhao, *Corros. Sci.,* 51(2009)1702.
7. T.Bellezze,G.Roventi and R.Fratesi, *Electrochim. Acta,* 49(2004)3005.
8. H. Tan, Y. M. Jiang, B. Deng, W.J.Gao and J.Li, *Nucl. Eng. Des.,* 241(2011)1421.

9. Y.H.Li, S.Z.Wang, X.Y.Tang, D.H.Xu, Y.Guo, J.Zhang and L.L.Qian, *Oxid. Met.,* 84(2015)509.
10. H. Meng, X. Hu and A. Neville, *Wear,* 263(2007)355.
11. K. M. Anwar Hossain, S. M. Easa and M. Lachemi, *Build. Environ.,* 44(2009)713.
12. S. Rivero, B. Chico and D. De la Fuente, *Rev. Metal. Madrid,* 43(2007)370.
13. F. Zhang, S.Chen, L.Dong, Y.Lei, T.Liu and Y.Yin, *Appl. Surf. Sci.,* 257(2011) 2587.
14. L.Freire, M.J.Carmezima and M.G.S.Ferreira, *Electrochim.Acta,* 56(2011)5280.
15. H.Luo, H.Z.Su, C.F.Dong and X.G.Li, *Appl. Surf. Sci.,* 400(2017)38.
16. S.M. Bhola, F.M. Alabbas, R. Bhola, J.R. Spear, B. Mishraa, D.L. Olson and A.E. Kakpovbia, *Eng. Fail. Anal.,* 36(2014)92.
17. F.M. Alabbas, S.M. Bhola, J.R. Spear, D.L. Olson and B. Mishra, *Eng. Fail. Anal.,* 33(2013)222.
18. K. Al-Muhanna and K. Habib, *Desalination,* 250(2010)404.
19. K.Q, R.F.Li, G.J.Wang, G.Z.Li, B.Liu and M.F.Wu, *J.Mater. Eng. Perform.,* 28(2019)287.
20. M.Kadowaki, I.Muto, H.Katayama, H.Masuda, Y.Sugawara and N.Hara, *Corros. Sci.,* 154(2019)159.
21. N.Sun, C. Wen, Z.L.Liu and X.Q.Liu, *Rare Metal Mat. Eng.,* 47(2018)860.